GSA Elections Begin 8 March

GSA TODAY

THE GEOLOGICAL SOCIETY OF AMERICA®

VOL. 32, NO. 3–4 | MARCH-APRIL 2022

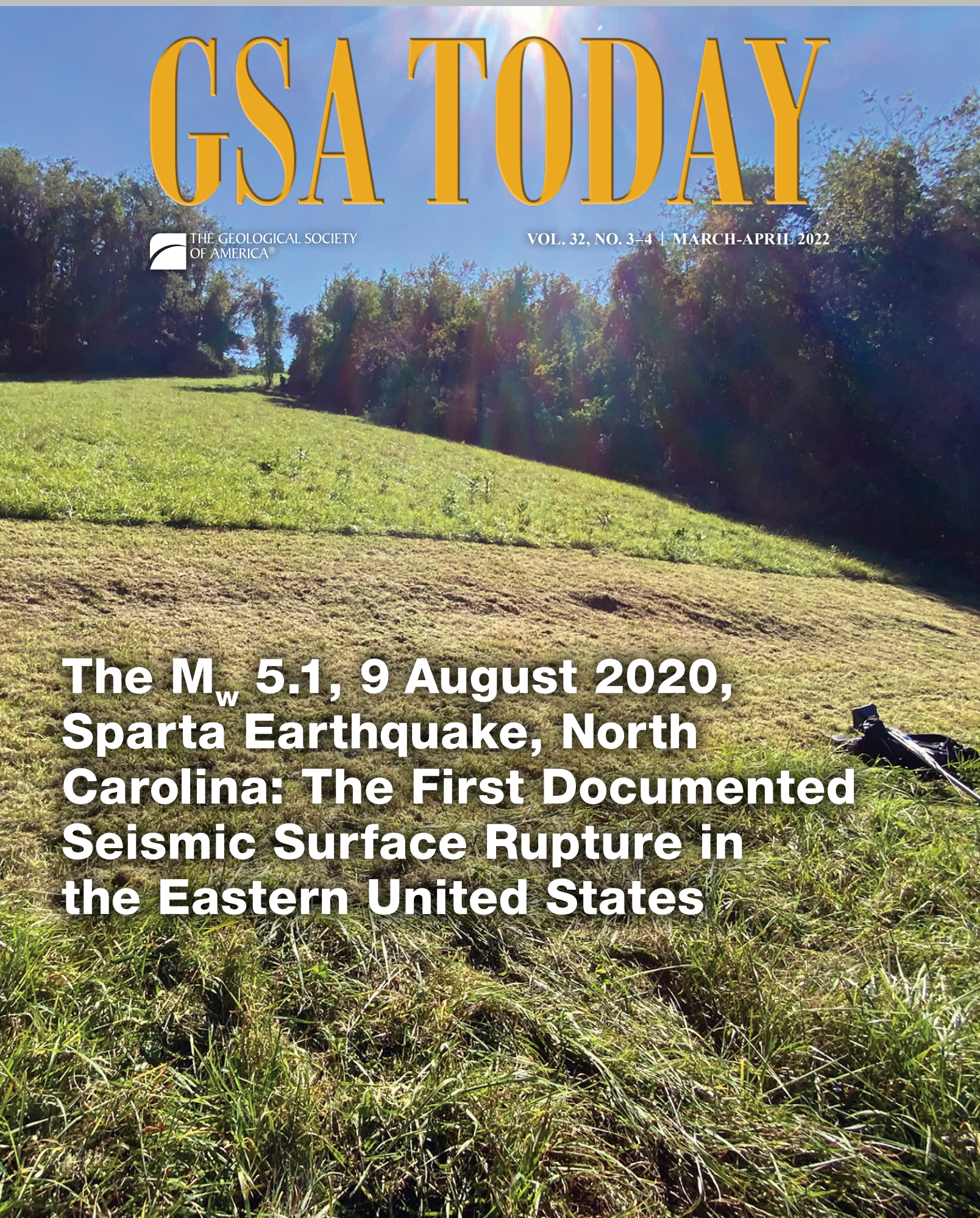

The M_w 5.1, 9 August 2020, Sparta Earthquake, North Carolina: The First Documented Seismic Surface Rupture in the Eastern United States

THE GEOLOGICAL SOCIETY OF AMERICA®

The M_w 5.1, 9 August 2020, Sparta Earthquake, North Carolina: The First Documented Seismic Surface Rupture in the Eastern United States

Paula M. Figueiredo, *Dept. of Marine, Earth and Atmospheric Sciences, North Carolina State University, Raleigh, North Carolina 27695, USA;* ***Jesse S. Hill,*** *North Carolina Geological Survey, Swannanoa, North Carolina 28778, USA;* ***Arthur J. Merschat,*** *U.S. Geological Survey, Florence Bascom Geoscience Center, Reston, Virginia 20192, USA;* ***Corey M. Scheip,*** *Dept. of Marine, Earth and Atmospheric Sciences, North Carolina State University, Raleigh, North Carolina 27695, USA, and North Carolina Geological Survey, Swannanoa, North Carolina 28778, USA;* ***Kevin G. Stewart,*** *Dept. of Geological Sciences, University of North Carolina at Chapel Hill, Chapel Hill, North Carolina 27599, USA;* ***Lewis A. Owen,*** *Dept. of Marine, Earth and Atmospheric Sciences, North Carolina State University, Raleigh, North Carolina 27695, USA;* ***Richard M. Wooten,*** *North Carolina Geological Survey, Swannanoa, North Carolina 28778, USA;* ***Mark W. Carter,*** *U.S. Geological Survey, Florence Bascom Geoscience Center, Reston, Virginia 20192, USA;* ***Eric Szymanski,*** *Dept. of Earth and Environmental Sciences, University of Michigan, Michigan 48109, USA;* ***Stephen P. Horton,*** *Center for Earthquake Research and Information, The University of Memphis, Memphis, Tennessee 38152, USA;* ***Karl W. Wegmann, DelWayne R. Bohnenstiehl,*** *Dept. of Marine, Earth and Atmospheric Sciences, North Carolina State University, Raleigh, North Carolina 27695, USA, and Center for Geospatial Analytics, North Carolina State University, Raleigh, North Carolina 27695, USA;* ***Gary W. Thompson,*** *North Carolina Geodetic Survey, Raleigh, North Carolina 27607, USA;* ***Anne Witt,*** *Virginia Dept. of Mines, Minerals and Energy, Virginia 22903, USA;* ***Bart Cattanach, Thomas Douglas,*** *North Carolina Geological Survey, Swannanoa, North Carolina 28778, USA*

ABSTRACT

At 8:07 a.m. EDT on 9 Aug. 2020 a M_w 5.1 earthquake located ~3 km south of Sparta, North Carolina, USA, shook much of the eastern United States, producing the first documented surface rupture due to faulting east of the New Madrid seismic zone. The co-seismic surface rupture was identified along a 2-km-long traceable zone of predominantly reverse displacement, with folding and flexure generating a scarp averaging 8–10-cm-high with a maximum observed height of ~25 cm. Widespread deformation south of the main surface rupture includes cm-dm–long and mm-cm–wide fissures. Two trenches excavated across the surface rupture reveal that this earthquake propagated to the surface along a preexisting structure in the shallow bedrock, which had not been previously identified as an active fault.

Surface ruptures by faulting are rarely reported for M <6 earthquakes, and hence the Sparta earthquake provides an opportunity to improve seismic hazard knowledge associated with these moderate events. Furthermore, this earthquake occurred in a very low strain rate intraplate setting, where earthquake surface deformation, regardless of magnitude, is sparse in time and rare to observe and characterize.

INTRODUCTION AND BACKGROUND

The M_w 5.1 Sparta earthquake was the largest in North Carolina in nearly 100 years (Stover and Coffman, 1993) and the strongest in the eastern United States since the 2011 M_w 5.8 Mineral, Virginia, earthquake. The maximum intensity was VI–VII (MMI) at Sparta and was widely felt across the eastern and central United States (USGS, 2020a). Most notably, the earthquake generated the first documentated co-seismic surface rupture by faulting in the eastern United States (Fig. 1).

Moderate (5 < M <6) to large (M ≥7) earthquakes in intraplate settings, such as the North American–Atlantic passive margin, are rare (Wolin et al., 2012). Notable earthquakes in the eastern and central U.S. include the 1755 Cape Ann (M 5.9; Ebel, 2006), the 1811–1812 New Madrid sequence (three ≥M7; Hough and Page, 2011), the 1886 Charleston, South Carolina (M 6.8–7.2; Chapman et al., 2016), and the 2011 Mineral, Virginia (M_w 5.8; Horton et al., 2015). Earthquakes occurring within the East Tennessee, central Virginia, Giles County, and coastal Charleston seismic zones contribute to North Carolina seismic hazard.

In the Blue Ridge physiographic province of North Carolina, historical earthquakes such as the 1861 Wilkesboro MMI V–VII, the 1916 M 5.2 Skyland, and the 1926 MMI V–VI Mitchell County had intensities comparable to the Sparta earthquake. However, there is insufficient information to infer which fault(s) generated them (Reinbold and Johnston, 1987; Stover and Coffman, 1993). The seismic catalog of Reinbold and Johnston (1987) documents 166 earthquakes since 1776, strong enough to be felt and interpreted to have their epicenters in or near North Carolina. However, instrumental seismicity records low magnitude (M ≤ 4) earthquakes, and in the Blue Ridge province, the mean hypocenter depth is 12 km (Bollinger et al., 1985).

The tectonic framework in the southern Appalachians preserves multiple Paleozoic orogenic events recorded by NE-trending regional structures (Hatcher et al., 2007). Crossing these structures are several poorly understood WNW to E-W topographic lineaments. Their genesis is speculated to result from early-to-mid-Mesozoic extension (e.g., Garihan and Ranson, 1992), Cenozoic mantle reorganization, which may account for Cenozoic regional uplift (Weems and Edwards, 2007; Gallen et al., 2013; Hill, 2018), or tectonic inheritance from Iapetian rifts (Thomas, 2011). In addition, some WNW lineaments have brittle deformation of unknown age and are roughly normal to

GSA Today, v. 32, https://doi.org/10.1130/GSATG517A.1.

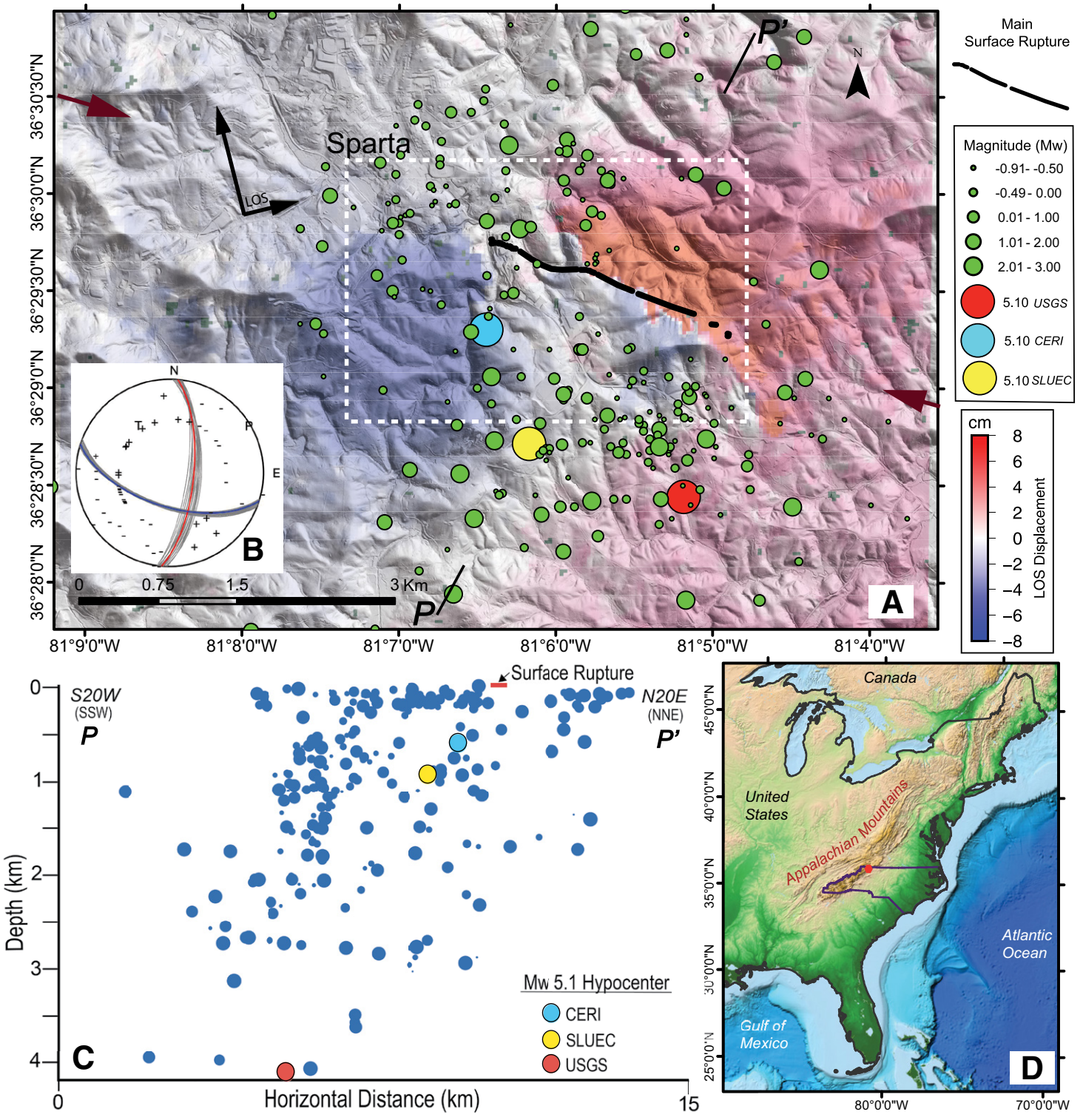

Figure 1. Location, earthquake sequence, and interferometric synthetic aperture radar interferogram for the Sparta earthquake. (A) Unwrapped phase interferogram overlaying a lidar-derived hillshade model with the main surface rupture (black line) and August 2020–February 2021 instrumental seismicity (circles; USGS catalog). Topographic lineament marked by brown arrows. Figure 2 location denoted by the dashed white rectangle. Line P–P' indicates the projection plane for seismicity. (B) Focal mechanism solution (Horton et al., 2021). (C) Projection of seismic sequence (USGS catalog) into a plane with azimuth N20°. (D) Location of the earthquake (red) in eastern North America, with North Carolina outlined. LOS—line of sight; CERI—Center for Earthquake Research and Information, University of Memphis; SLEUC—Saint Louis University Earthquake Center.

the NE-SW to ENE-WSW regional S_{Hmax} (Snee and Zoback, 2020), favoring them as potentially seismogenic. However, these WNW-trending structures are not included in the USGS Quaternary Faults or U.S. Seismic Source Characterization for Nuclear Facilities databases (Crone and Wheeler, 2000; Machette et al., 2004; U.S. Nuclear Energy Regulatory Commission, 2012).

THE SPARTA EARTHQUAKE

The surface rupturing M_w 5.1 Sparta earthquake occurred on a WNW-striking previously unknown structure, now named the Little River fault (Hill et al., 2020). The main event generated peak ground accelerations of at least 0.2 g with an MMI of VI–VII in Sparta (USGS, 2020a). Roads, utility lines, and masonry structures were damaged, including the collapse of walls and chimneys and the cracking and shifting of foundations, causing North Carolina's governor to declare a local state of emergency and the North Carolina General Assembly to provide U.S.$24M for earthquake recovery (Office of State Budget and Management, 2020, pers. comm.). Fortunately, there were no casualties or significant damage to major infrastructures.

The mainshock hypocenter and focal mechanism have been estimated independently by several groups. Horton et al. (2021) at the Center for Earthquake Research and Information, University of Memphis (CERI), calculated a first-motion focal mechanism consistent with a N108°-striking 60° SW-dipping nodal plane, with a 24° rake (Fig. 1B) and a best-fitting centroid depth of 0.6 km based on modeling regional waveforms and an epicenter location (36.488° N, 81.106° W) using a grid search procedure. The Saint Louis University Earthquake Center calculated a centroid depth of 1 km with a N115°, 50° SW nodal plane and rake of 40° based on best-fit modeling of regional waveforms (SLUEC, 2020). Analysis by SLUEC (2020) and Horton et al. (2021) yield similar results consistent with a shallow (<1 km) left-lateral reverse rupture on a SW-dipping plane. These results, however, differ from the preferred USGS solution, which places the event deeper (4.1 ± 1.8 km), with a nodal plane striking N176°, 48° W and a rake of 136° (USGS, 2020b). The earthquake sequence started with eight foreshocks with M_w 1.8–2.6 during the 24 h before the mainshock, followed by at least 300 aftershocks over the next six months, the largest being an M_w 2.9 on 11 August. The aftershock sequence was mainly recorded with a real-time broadband seismic array installed by CERI 48 h after the main shock. Most aftershocks were M_w <1.5, shallower than 3 km, and distributed across a 40-km^2 elliptical area with its major axis trending NW to WNW (USGS Catalog August–February 2021; Fig. 1A). The plotted aftershock hypocenters projected onto a cross section normal to the rupture suggest that the earthquake sequence is associated with a SW-dipping structure (Fig. 1C).

RECOGNITION OF THE SURFACE DEFORMATION

The recognition and mapping of a surface rupture trending ~N110° began on the day of the earthquake and continued for several months. The collection of uncrewed aerial systems (UAS) imagery and processing of digital terrain models aided field mapping, highlighting minor topographic changes along the surface rupture and identifying small-scale deformation features (Figs. 2B–2F). In addition, the co-seismic scarps were surveyed with a real-time kinematic global positioning system to measure displacements.

A preliminary interferometric synthetic aperture radar (InSAR) analysis was conducted using ascending Sentinel-1A imagery acquired a day before the Sparta earthquake (8 August) and Sentinel 1B imagery acquired six days later (l4 August). Despite areas of poor coherence, the unwrapped interferogram delineates an area of deformation of ~20 km^2 (Fig. 1A). An irregular contact between a positive and negative line-of-sight (LOS) trends ~N125° for ~3-km, roughly coincident with the mapped co-seismic surface rupture. The southern block has a negative LOS (movement away from the ENE-looking satellite), while the northern block has a positive LOS (movement toward the satellite). These patterns are consistent with left-lateral reverse motion occurring along the SW-dipping nodal plane identified in the focal mechanism.

In the hanging wall, located ~300 m and 600 m from the main surface rupture, the *Alleghany 13* and *Funeral* geodetic monuments surveyed by the North Carolina Geodetic Survey in September–November 2020 moved 19.7 cm to the ESE and 5.7 cm to the ENE, respectively, and *Alleghany 13* rose 15 cm (Fig. 2A). The geodetic monument *Alleghany 15*, located ~600 m north of the main surface rupture shifted 7.8 cm toward the SW. These movements are consistent with the determined focal mechanism and InSAR analysis.

Along the central portion of the surface rupture, several 250 MHz ground-penetrating radar (GPR) profiles were acquired perpendicular to the surface rupture. The GPR profiles consistently show sub-horizontal reflectors in the upper ~4 m crossed by a few 20–30° south-dipping reflectors. While this is the expected co-seismic rupture geometry, one dipping reflector projects to the surface a few meters to the north of the surface rupture (Fig. 3G).

GEOLOGICAL ANALYSIS OF SURFACE DEFORMATION

No major ground cracking was evident near the epicenter. The majority of the surface rupture is located to the south and southeast of Sparta, and north of U.S. Route 21, stretching for ~2 km and across a generally <25-m-wide zone. The most prominent features and primary evidence of surface rupture are straight ten to hundreds of meters long, ~N110°-trending occasionally en échelon ground ruptures. Along the rupture, a co-seismic topographic step, formed by reverse scarps and folding/flexure of the topography, has an average height of 8–10 cm and a maximum of ~25 cm. The southern block is consistently uplifted. The surface rupture has four sections (A to D in Fig. 2A):

1. **Greenway Drive industrial park (section A):** South of downtown Sparta several ground fissures (crossing U.S. Route 21) and small scarps align in strike for a distance of ~300 m as they cross the industrial park at Greenway Drive. The structures trend N100–110°, and some exhibit a subtle right-stepping en échelon pattern. The scarps are single or multiple minor steps, building to a ~20 cm high maximum (Figs. 2B–2D). Folding associated with the uplift caused extension at the top of the hanging wall with oblique fissures and cracks. Evidence for lateral displacement is minor, and no marker was laterally displaced across the rupture trace. Several buildings were moderately damaged in the industrial park, particularly those on the surface rupture. Many secondary ground fissures were induced by ground shaking to the south and west of the industrial park (Fig. 2A).
2. **Little River valley (section B):** The rupture crosses the Little River valley for ~500 m along a steep and densely vegetated slope that hampers features

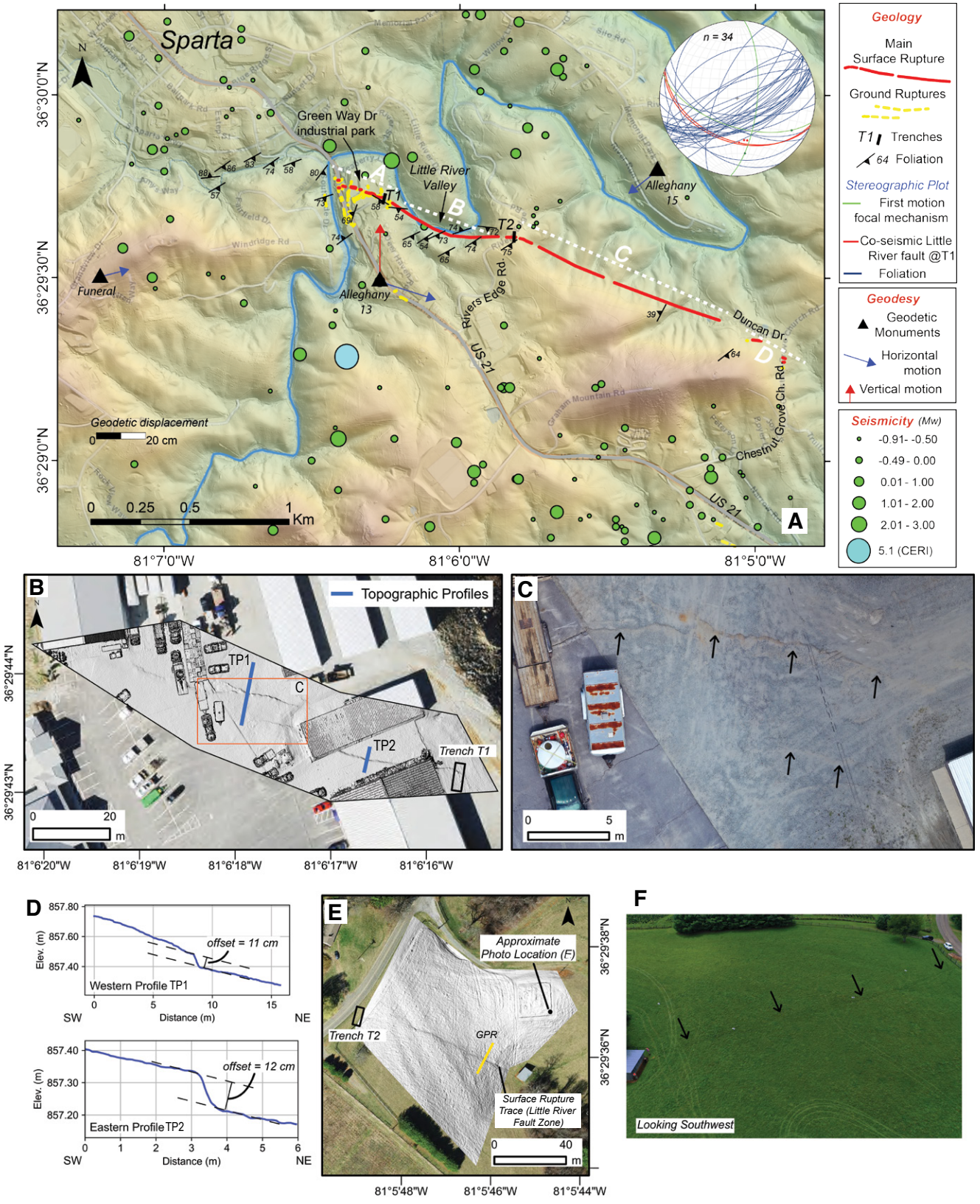

Figure 2. Co-seismic main surface rupture along the newly identified Little River fault. (A) Main surface and ground ruptures, locations of displaced geodetic monuments, and earthquake sequence. Topographic map overlaying digital elevation model (DEM) and hillshade. White dashed lines indicate the surface rupture sections (A–D) described in the text. The stereogram displays the focal mechanism (green), measured fault (red), and foliation (blue) orientations. Location of 2A provided by inset in Figure 1A. (B and C) Greenway Drive industrial park, uncrewed aerial systems (UAS) imagery in B is overlain by UAS-DEM with topographic profiles TP1 and TP2 (blue lines) along the surface rupture. The red rectangle is the inset area of (C), where arrows highlight surface rupture trace. (D) Topographic profiles TP1 and TP2 (VE = 10×) extracted from UAS-DEM. (E and F) Rivers Edge Road, UAS imagery in E is overlain by UAS-DEM and includes the location of ground penetrating radar profile line 02 presented in Figure 3G. Arrows in (F) highlight the surface rupture crossing the field.

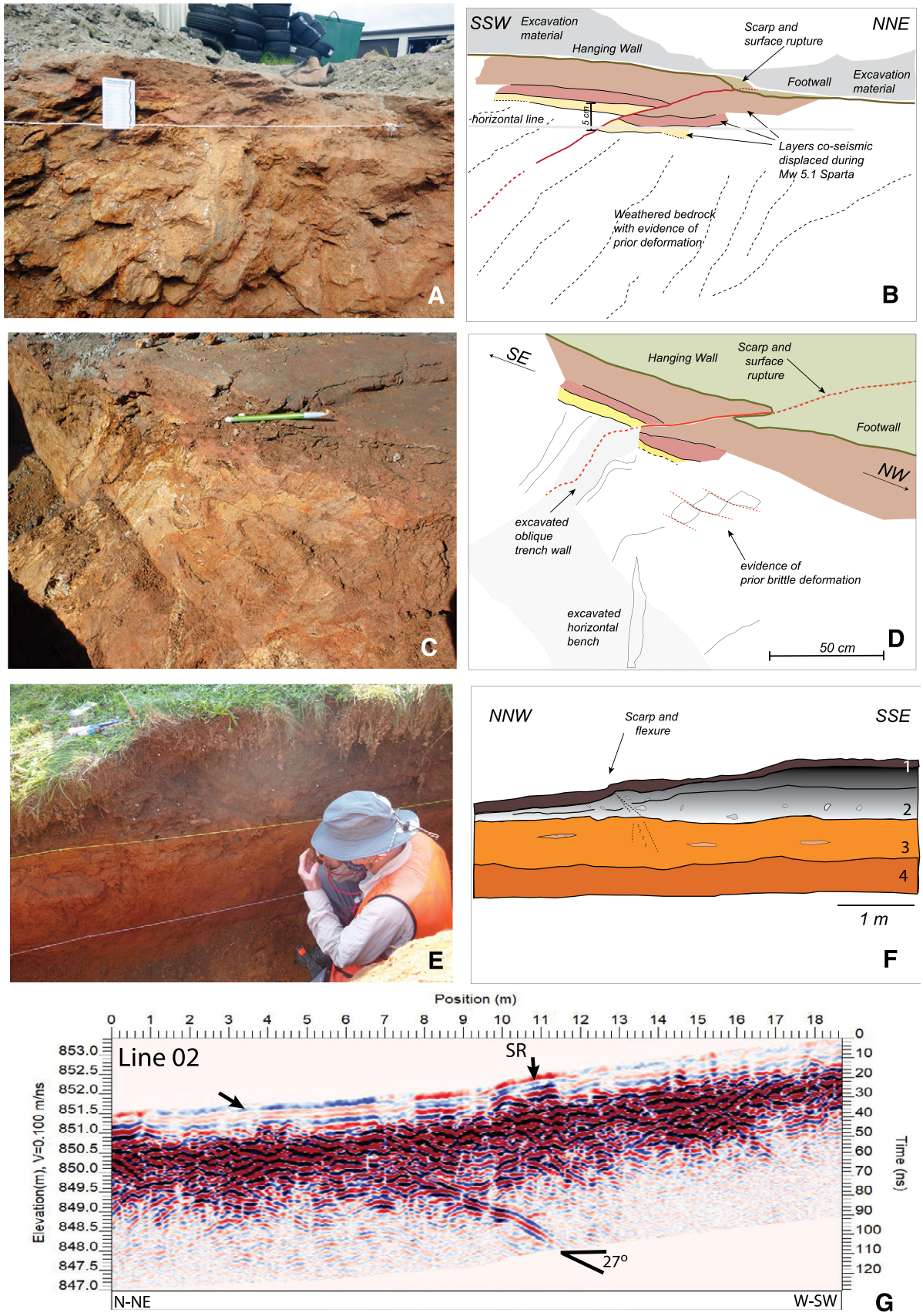

Figure 3. Views and interpretations of trenches and ground penetrating radar (GPR) results. (A and B) T1 southern wall exhibiting reverse faulting of upper layers by a low-angle plane, rooted in a preexistent fabric in metamorphic bedrock. (C and D) The T1 southern wall highlights previous ductile and brittle deformation. (E) View of the scarp and colluvium in the eastern wall of T2. (F) Fault trench log for the eastern wall of T2 showing flexure with no faulting. (G) GPR Line 02 (location in Fig. 2E), highlighting a low-angle south-dipping reflector. SR—surface rupture.

recognition. We identified two small N110°-trending fissures in the south river bank, with 2–3 cm of reverse vertical offset. Minor rockfall on the southern slope and a small liquefaction feature in a sand bar on the northern riverbank were also documented.

3. **Rivers Edge Road (section C):** An ~8-cm-high rupture scarp, trending ~N90°, crossed Rivers Edge Road, causing buckling of the road and breakage of a buried water pipe (Figs. 2E–2F). Eastward, the surface rupture crosses a north-facing slope in open fields and forest patches, striking ~N110° with a linear and continuous trace. The topographic step is single or complex, with heights varying between 5 and ~25 cm. It was trackable for ~1,100 m until the scarp and fissures stopped being detectable due to dense vegetation.
4. **Chestnut Grove Church Road (section D):** The surface rupture is subdued as it continues from Duncan Drive to Chestnut Grove Church Road. Small fissures and WNW-trending 3–4-cm-high steps occur in a cattle path close to Duncan Drive. Following the rupture strike N110° to Chestnut Grove Church Road, extensional co-seismic fissures broke the road into several decameter blocks, which have a similar geometry to older cracks in the asphalt. These co-seismic fissures suggests that preexisting mass wasting–related features were activated during the earthquake. We interpret these as minor deformation along the eastward rupture termination.

South of U.S. Route 21 and southwest of Sparta, co-seismic deformation not related to the main rupture trace, expressed by ground fissures in less consolidated material in road cuts and riverbanks, resulted from ground shaking or translational sliding (Fig. 2A). Near Little River, riverbank fissures are subparallel with cm-dm–long and mm-cm–wide openings. At an industrial parking lot (3238 U.S. Route 21, Glade Valley, North Carolina), co-seismic fissures extend for several m with mm-to-cm openings, exhibiting shortening and extensional displacement. These features are likely due to co-seismic deformation along several preexisting pavement discontinuities formed by earlier downslope processes and differential compaction in artificial fills.

FAULT TRENCHING AND SUBSURFACE ANALYSIS

We excavated two trenches to investigate the earthquake deformation (Figueiredo et al., 2020). Trench T1 was excavated three days after the mainshock at the Greenway Drive industrial park (section A) at the tip of a rupture segment (Figs. 2A and 3A–3D). A ~5-m-long and ~1.2-m-deep trench exposed weathered Neoproterozoic to Ordovician metasedimentary bedrock of the Ashe Metamorphic Suite overlain by northward-thickening horizontal layers of clay and sand construction fill. A thrust fault is recognized in the upper few dm of the trench displacing surficial fill deposits ~10 cm along a fault plane (N100°, 19° S) with 4-cm vertical displacement of the southern hanging wall, forming a small, very well-preserved scarp. The low-angle fault roots into weathered bedrock ~20 cm into a steeper preexisting plane (N115°, 45° S) interpreted to be associated with the Paleozoic fabric. Primarily dip-slip slickenlines were identified in the low-angle and steeper fault surfaces, although oblique slickenlines were observed near the surface in folded materials of the scarp (Hill et al., 2020). Small excavations within the industrial park across minor scarps corroborate reverse faulting and cumulative co-seismic vertical displacements of up to 10 cm. Moreover, markers in the pavement across the fault trace were not laterally displaced. Older fault gouge with manganese-coated surfaces and breccia in the weathered bedrock indicates brittle deformation, with dip-slip slickenlines. The age of the brittle deformation is unknown.

Trench T2 (~1.3-m deep and ~10-m long) was opened along the side of Rivers Edge Road across an ~8-cm-high scarp next to a buckled road and broken water pipe (Figs. 2A and 3E–3F). The excavation exposed two clay-rich colluvial units (2 and 3) and saprolite (4), which were not displaced by a fault despite being positioned across the scarp. The upper colluvium (1) was gently warped; however, this folding was not observed in the lower colluvium or saprolite. The absence of faulting despite the evident compression was corroborated by a 250 MHz GPR profile parallel to T2 interpreted as recording minimal-to-no stratigraphic disturbance in the upper 4 m. We argue that T2 is located in a compressional step-over.

There was no clear evidence for cumulative Quaternary deformation prior to the 2020 earthquake due to a lack of additional Quaternary markers at depth in T1. Nonetheless, both trenches unequivocally demonstrate surface deformation caused by an active fault.

RELATION TO TECTONIC FRAMEWORK AND GEOMORPHOLOGY

The focal mechanism, InSAR interferograms, field observations, and aftershock sequence provide evidence supporting a SSW-dipping seismogenic fault. The surface ruptures are ~N110°, similar to the strike of the south-dipping nodal plane for the first motion moment tensor solutions and the InSAR unwrapped interferograms. None of these matches mapped tectonic structures in the Sparta area (Rankin et al., 1972; NCGS, 1985; Merschat et al., 2020). However, the Little River fault is subparallel to the Boone and Mills Gap faults, located 50 and 150 km to the southwest, respectively (Wooten et al., 2010; Hill, 2018). Hill (2018) argued that WNW lineaments in North Carolina are likely brittle Cenozoic structures. The surface rupture is located along a subtle ~10-km-long WNW-ESE–trending topographic lineament visible in digital elevation models and centered on the fault zone (Fig. 1A).

DISCUSSION

The Sparta earthquake is unusual for eastern North America and worldwide because $4.5 < M_w < 5.5$ earthquakes rarely produce surface ruptures. It was also unexpected, occurring along an unknown structure trending oblique to the regional NE-SW structural trend and triggered at shallower depths than regional seismicity.

The fault identified in trench T1 (N115°, 45°S) was interpreted as reactivation of a foliation plane (Fig. 2A). We argue that the foliation parallel to the active fault in T1 could be locally rotated due to brittle deformation, similar to anomalous WNW rotated foliation observed in the Mills Gap fault zone (Wooten et al., 2010). Trench T2 is placed at a compressional step-over without evidence of faulting. Nonetheless, GPR profiles acquired 20 m to the east of T2 and along an ~600-m segment consistently show a low-angle south-dipping reflector (Fig. 3G). This reflector projects to the surface a few meters north of the co-seismic scarp, where ground deformation was not recognized. We suggest that this reflector may be (1) related to an older earthquake structure or (2) the result of deformation partitioning on an unidentified complex set of structures during the 2020 earthquake.

The strike of the seismogenic structure inferred from seismology and remote sensing is consistent with field observations. However, and interestingly, the kinematics

are different from the observed slip. The focal mechanism derived from waveform analysis and the InSAR unwrapped interferogram indicate oblique-reverse motion. Geodetic monuments were displaced differently on the hanging wall and footwall supporting a left-lateral and reverse motion. In contrast, the geologic field evidence suggests predominantly reverse faulting and associated folding along a low-angle (~20°) fault plane that roots in a steeper preexistent fabric (~50°). This discrepancy may indicate complex strain partitioning or a change of slip during the earthquake. The initial, deep rupture may be predominantly strike-slip, possibly along a steeper structure with subsequent up-dip failures on shallower preexisting planar discontinuities in the bedrock accommodating most of the reverse component. Slip variations during an earthquake rupture are recognized from recent and historical earthquakes (Kearse and Kaneko, 2020). Further research is needed to understand slip partioning associated with the Sparta earthquake.

Eastern North American earthquakes commonly have complex ruptures. According to Horton et al. (2015), significant earthquakes such as the 1988 M_w 5.9 Saguenay and 1989 M_w 6.0 Ungava, both in Quebec, and the 2011 M_w 5.8 Mineral, Virginia, event had large local stress drops and complex ruptures that evolved spatially and temporally. The 2011 Mineral earthquake had three subevents, with most of the seismic moment release occurring at a depth of 8 km as the earthquake rupture propagated from SW to NE along strike and up-dip (Chapman, 2013; Hartzell et al., 2013; Horton et al., 2015). The Sparta earthquake had a shallow centroid depth and moment release more favorable for surface rupture.

The regional S_{Hmax} is NE-SW to ENE-WSW (Snee and Zoback, 2020), consistent with an oblique-reverse focal mechanism and overall reverse fault characteristics. Several processes can increase the stress field and trigger seismicity, including glacioisostatic adjustments, loading/unloading of sediments or water, and static stress changes; however, none of these apply to the Sparta region. Walsh et al. (2015) analyzed the Coulomb static stress transfer during the 2011 Mineral earthquake, and except for an area in the range of 10 km from the main event, stress changes are negligible (~1 mbar) and much less than the values needed to trigger earthquakes at a regional scale. Since Sparta is located ~300 km from the 2011 Mineral seismic area, relevant stress perturbations from the 2011 earthquake are unlikely to be the cause. The Sparta focal mechanism (SLUEC, 2020; Horton et al., 2021) is similar to the ones obtained for the Giles County, Virginia, seismic zone, located ~100 km to the north-northeast. Across a six-year survey, Munsey and Bollinger (1985) calculated several predominately strike-slip moment tensor solutions where the left-lateral solutions have an ESE trend dipping steeply to the south, similar to the 2020 Sparta earthquake.

In intraplate settings, recognizing active structures and quantifying their deformation rates for seismic hazard can be challenging when seismicity is diffuse and infrequent, with long periods of quiescence spanning $10^{5–6}$ years (e.g., Clark et al., 2012). The recognition and documentation of moderate earthquakes with surface rupture, like that of the 2020 Sparta M_w 5.1 earthquake, has increased recently (e.g., King et al., 2019; Ritz et al., 2020), likely due to the increasing knowledge and availability of remote sensing methods. These earthquakes provide direct evidence of seismicity that is generally poorly expressed or misunderstood in the paleoseismologic record. In the case of the Sparta earthquake, the application of the magnitude-surface deformation empirical relationships (e.g., Wells and Coppersmith, 1994) would support a larger magnitude event. This discrepancy indicates that paleoseismology data may be underestimating seismic hazard for certain cases. Thus, documentation of surface deformation generated from moderate seismicity is meaningful and relevant for seismic hazard assessment, not only for intraplate settings.

CONCLUSIONS

The moderate M_w 5.1 Sparta earthquake produced complex oblique reverse-faulting with surface rupture, the first recorded earthquake to do so across the eastern United States. The seismogenic source strikes WNW and dips SW, and instrumental data support a left-lateral earthquake with reverse slip. However, field investigations of the main surface rupture, document predominantly reverse slip, controlled by a preexisting planar structure, inferred to show brittle deformation of probable Cenozoic age. This structure, now recognized and named Little River fault, is possibly part of a WNW-ESE set of lineaments inferred to have Cenozoic activity that crosses the dominant NE-SW Appalachian structural grain. The shallow (~0.6–1.0 km) hypocenter promoted surface rupture. Left-lateral reverse motion on a WNW-ESE–trending fault is consistent with the regional stress field, with S_{Hmax} oriented NE-SW to ENE-WSW. The occurrence of Quaternary activity preceding the 2020 Sparta earthquake has yet to be determined.

Two moderate earthquakes (2011 M_w 5.8 Mineral and 2020 M_w 5.1 Sparta), occurred in eastern North America during the past decade, causing disruption and economic loss. These occurred along structures not included in any database as potentially active, suggesting that the regional seismic hazard may be underestimated.

ACKNOWLEDGMENTS

We thank the National Science Foundation for supporting this research (EAR-2102530, support from Tectonics, Geomorphology and Land Use Dynamics, and the Geophysics programs) and the people of Alleghany County in North Carolina for providing access to their lands, particularly Ann Downing and the business owners within the Greenway Drive industrial park. U.S. Geological Survey research supported by the National Cooperative Geologic Mapping Program and Earthquake Hazards Program. Thanks to Sarah Wells and Ashley Lynn for field assistance and Daria Khashchevskaya for help with graphics, and to Thomas Pratt and J. Wright Horton, Jr., and two anonymous reviewers for their comments, which greatly improved this manuscript. Any use of trade, firm, or product names is for descriptive purposes only and does not imply endorsement by the U.S. government.

REFERENCES CITED

Bollinger, G.A., Chapman, M.C., Sibol, M.C., and Costain, J.K., 1985, An analysis of the focal depths in the Southeastern U.S.: Geophysical Research Letters, v. 12, no. 11, p. 785–788, https://doi.org/10.1029/GL012i011p00785.

Chapman, M.C., 2013, On the rupture process of the 23 August 2011 Virginia earthquake: Bulletin of the Seismological Society of America, v. 103, no. 2a, p. 613–628, https://doi.org/10.1785/0120120229.

Chapman, M.C., Beale, J.N., Hardy, A.C., and Wu, Q., 2016, Modern seismicity and the fault responsible for the 1886 Charleston, South Carolina, earthquake: Bulletin of the Seismological Society of America, v. 106, no. 2, p. 364–372, https://doi.org/10.1785/0120150221.

Clark, D., McPherson, A., and Van Dissen, R., 2012, Long-term behaviour of Australian stable continental region (SCR) faults: Tectonophysics, v. 566–567, p. 1–30, https://doi.org/10.1016/j.tecto.2012.07.004.

Crone, A.J., and Wheeler, R.L., 2000, Data for Quaternary faults, liquefaction features, and possible tectonic features in the Central and Eastern United States, east of the Rocky Mountain front: U.S. Geological Survey Open-File Report 00-260, 332 p., https://doi.org/10.3133/ofr00260.

Ebel, J.E., 2006, The Cape Ann, Massachusetts Earthquake of 1755: A 250th Anniversary Perspective:

Seismological Research Letters, v. 77, no. 1, p. 74–86, https://doi.org/10.1785/gssrl.77.1.74.

Figueiredo, P., Carter, M.W., Cattanach, B., Douglas, T., Hill, J., Kirby, E., Korte, K., Lynn, A., Merschat, A., Owen, L., Scheip, C., Stewart, K., Wells, S., and Wooten, R., 2020, Preliminary observations of M_w 5.1 Sparta (North Carolina) surface deformation—A first documented M_w 5 instrumental earthquake surface rupture in Eastern U.S.A.?: Southern California Earthquake Center Annual Meeting, contribution 10753, https://www.scec.org/meetings/2020/am/poster/007.

Gallen, S.F., Wegmann, K.W., and Bohnenstiehl, D.W.R., 2013, Miocene rejuvenation of topographic relief in the southern Appalachians: GSA Today, v. 23, p. 4–10, https://doi.org/10.1130/GSATG163A.1.

Garihan, J.M., and Ranson, W.A., 1992, Structure of the Mesozoic Marietta-Tryon graben, South Carolina and adjacent North Carolina, *in* Bartholomew, M.J., Hyndman, D.W., Mogk, D.W., and Mason, R., eds., Basement Tectonics 8: Dordrecht, Springer, Proceedings of the International Conferences on Basement Tectonics, v. 2, https://doi.org/10.1007/978-94-011-1614-5_36.

Hartzell, S., Mendoza, C., and Zeng, Y., 2013, Rupture model of the 2011 Virginia, earthquake from teleseismic and regional waveforms: Geophysical Research Letters, v. 40, p. 5665–5670, https://doi.org/10.1002/2013GL057880.

Hatcher, R.D., Jr., Bream, B.R., and Merschat, A.J., 2007, Tectonic map of the southern and central Appalachians: A tale of three orogens and a complete Wilson cycle, *in* Hatcher, R.D., Jr., Carlson, M.P., McBride, J.H., and Martínez Catalán, J.R., eds., 4-D Framework of Continental Crust: Geological Society of America Memoir 200, p. 595–632, https://doi.org/10.1130/2007.1200(29).

Hill, J.S., 2018, Post-orogenic uplift, young faults and mantle reorganization in the Appalachians [Ph.D. dissertation]: The University of North Carolina at Chapel Hill, 130 p., https://doi.org/10.17615/rnrd-0d82.

Hill, J.S., Cattanach, B.L., Douglas, T.J., Figueiredo, P.M., Kirby, E., Korte, D.M., Lynn, A.S., Merschat, A.J., Owen, L.A., Scheip, C., Stewart, K.G., Wells, S.B., and Wooten, R.M., 2020, Surface rupture of the Little River fault in response to the August 9, 2020 M_w 5.1 earthquake near Sparta, North Carolina: 2020 Southern California Earthquake Center Annual Meeting, contribution 10742, https://www.scec.org/meetings/2020/am/poster/006.

Horton, J.W., Jr., Chapman, M.C., and Green, R.A., 2015, The 2011 Mineral, Virginia, earthquake, and its significance for seismic hazards in eastern North America—Overview and synthesis, *in* Horton, J.W., Jr., Chapman, M.C., and Green, R.A., eds., The 2011 Mineral, Virginia, Earthquake, and Its Significance for Seismic Hazards in Eastern North America: Geological Society of America Special Paper 509, p. 1–25, https://doi.org/10.1130/2015.2509(01).

Horton, S., Withers, M., Cramer, C., and Withers, H., 2021, Source Parameters of the M5.1 Sparta, NC Earthquake of August 9, 2020, Seismological Society of America Annual Meeting: Seismological Research Letters, v. 92, 2B, p. 1439.

Hough, S.E., and Page, M., 2011, Towards a consistent model for strain accrual and moment release in the New Madrid, Central US seismic zone: Journal of Geophysical Research, Solid Earth, v. 116, B03311, https://doi.org/10.1029/2010JB007783.

Kearse, J., and Kaneko, Y., 2020, On-fault geological fingerprint of earthquake rupture direction: Journal of Geophysical Research, Solid Earth, v. 125, https://doi.org/10.1029/2020JB019863.

King, T.R., Quigley, M., and Clark, D., 2019, Surface-rupturing historical earthquakes in Australia and their environmental effects: New insights from re-analyses of observational data: Geosciences, v. 9, 408, https://doi.org/10.3390/geosciences9100408.

Machette, M.N., Haller, K.M., and Wald, L.A., 2004, Quaternary fault and fold database for the nation: U.S. Geological Survey Fact Sheet, 2004-3033, https://doi.org/10.3133/fs20043033.

Merschat, A.J., Carter, M.W., Scheip, C.M., Wooten, R.M., Owen, L.A., Douglas, T.J., Figueiredo, P., Cattanach, B.L., Stewart, K., Hill, J., and Witt, A., 2020, Surface rupture from the 9 August 2020, M_w 5.1 Sparta, North Carolina earthquake and connections with bedrock geology: Geological Society of America Abstracts with Programs, v. 52, no. 6, https://doi.org/10.1130/abs/2020AM-361227.

Munsey, J.W., and Bollinger, G.A., 1985, Focal mechanism analyses for Virginia Earthquakes (1978–1984): Bulletin of the Seismological Society of America, v. 75, no. 6, p. 1613–1636, https://doi.org/10.1785/BSSA0750061613.

North Carolina Geological Survey, 1985, Geologic map of North Carolina: Raleigh, North Carolina Department of Natural Resources and Community Development, Division of Land Resources, scale 1:500,000.

Rankin, D.W. Espenshade, G.H., and Neuman, R.B., 1972, Geological map of the west half of the Winston-Salem quadrangle, North Carolina, Virginia and Tennessee: U.S. Geological Survey Miscellaneous Geologic Investigations, Map I-709-A, scale: 1:250, 000.

Reinbold, D.J., and Johnston, A.C., 1987, Historical Seismicity in the Southern Appalachian Seismic Zone: U.S. Geological Survey Open-File Report 87-433 (contract report).

Ritz., J.-F., Baize, S., Ferry, M., Larroque, C., Audin, L., Delouis, B., and Mathot, E., 2020, Surface rupture and shallow fault reactivation during the 2019 M_w 4.9 Le Teil earthquake, France: Communications Earth & Environment, https://doi.org/10.1038/s43247-020-0012-z.

SLUEC, 2020, Saint Louis University Earthquake Center: http://www.eas.slu.edu/eqc/eqc_mt/MECH.NA/20200809120737/index.html (accessed 21 Feb. 2021).

Snee, J.-E.-L., and Zoback, M.D., 2020, Multiscale variations of the crustal stress field throughout North America: Nature Communications, v. 11, 9 p., https://doi.org/10.1038/s41467-020-15841-5.

Stover, C.W. and Coffman, J.L., 1993, Seismicity of the United States, 1568–1989: U.S. Geological Survey Professional Paper 1527, 417 p., https://doi.org/10.3133/pp1527.

Thomas, W.A., 2011, The Iapetan rifted margin of southern Laurentia: Geosphere, v. 7, no. 1, p. 97–120, https://doi.org/10.1130/GES00574.1.

Walsh, L.S., Montési, L.G.J., and Marin, A.J., 2015, Coulomb stress transfer and modeled permanent vertical surface deformation from the August 2011, Mineral, Virginia, earthquake, *in* Horton, J.W., Jr., Chapman, M.C., and Green, R.A., eds., The 2011 Mineral, Virginia, Earthquake, and Its Significance for Seismic Hazards in Eastern North America: Geological Society of America Special Paper 509, p. 305–329, https://doi.org/10.1130/2015.2509(18).

Weems, R.E., and Edwards, L.E., 2007, Post-middle Miocene origin of modern landforms in the eastern Piedmont of Virginia: Stratigraphy, v. 4, p. 35–48.

Wells, D., and Coppersmith, K., 1994, New empirical relationships among magnitude, rupture length, rupture width, rupture area and surface displacement: Bulletin of the Seismological Society of America, v. 84, no. 4, p. 974–1002.

Wolin, E., Stein, S., Pazzaglia, F., Meltzer, A., Kafka, A., and Berti, C., 2012, Mineral, Virginia, earthquake illustrates seismicity of a passive-aggressive margin: Geophysical Research Letters, v. 39, L02305, https://doi.org/10.1029/2011GL050310.

Wooten, R.M., Cattanach, B.L., Gillon, K.A., and Bozdog, G.N., 2010, Geology of the Mills Gap area, Buncombe County, NC: North Carolina Geological Survey Report of Special Investigation 2010-09-30, Technical Memorandum to the U.S. Environmental Protection Agency, USGS, and the NC Department of Environment and Natural Resources, Division of Waste Management, 19 p., 2 plates.

USGS, 2020a, U.S. Geological Survey: https://earthquake.usgs.gov/earthquakes/eventpage/se60324281/map?dyfi-responses-10km=true&shakemap-intensity=false, (accessed 18 Dec. 2020).

USGS, 2020b, U.S. Geological Survey: https://earthquake.usgs.gov/earthquakes/eventpage/se60324281/moment-tensor (accessed 15 Feb. 2021).

U.S. Nuclear Regulatory Commission, 2012, Central and Eastern United States Seismic Source Characterization for Nuclear Facilities, NUREG-2115, 364 p., https://www.nrc.gov/docs/ML1204/ML12048A804.pdf (accessed 6 May 2021).

Manuscript received 4 June 2021
Revised manuscript received 4 Jan. 2022
Manuscript accepted 5 Jan. 2022